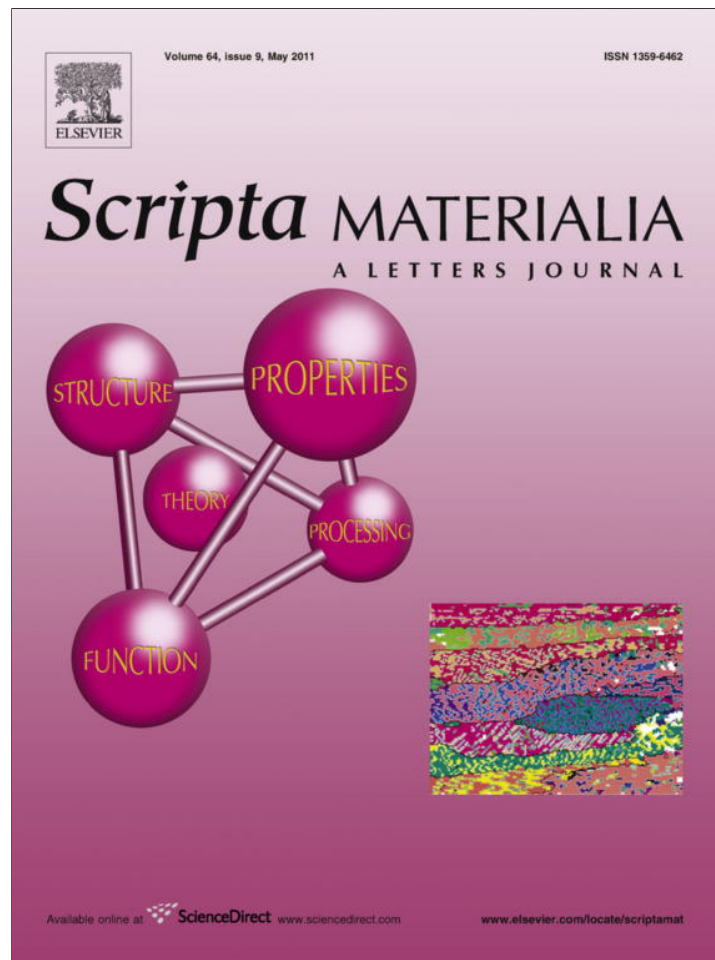


Provided for non-commercial research and education use.
Not for reproduction, distribution or commercial use.



This article appeared in a journal published by Elsevier. The attached copy is furnished to the author for internal non-commercial research and education use, including for instruction at the authors institution and sharing with colleagues.

Other uses, including reproduction and distribution, or selling or licensing copies, or posting to personal, institutional or third party websites are prohibited.

In most cases authors are permitted to post their version of the article (e.g. in Word or Tex form) to their personal website or institutional repository. Authors requiring further information regarding Elsevier's archiving and manuscript policies are encouraged to visit:

<http://www.elsevier.com/copyright>



Boron clustering in implanted NiSi

A. Portavoce,^{a,*} I. Blum,^a D. Mangelinck,^a K. Hoummada,^b L. Chow,^c V. Carron^d and J.L. Lábár^e

^aCNRS, IM2NP, Faculté des Sciences de Saint-Jérôme Case 142, 13397 Marseille, France

^bAix-Marseille Université, IM2NP, Faculté des Sciences de Saint-Jérôme Case 142, 13397 Marseille, France

^cDepartment of Physics, University of Central Florida, Orlando, FL 32816, USA

^dCEA-LETI, MINATEC, 17 rue des Martyrs, 38054 Grenoble Cedex 9, France

^eResearch Institute for Technical Physics and Materials Science, Konkoly-Hege u. 29-33, 1121 Budapest, Hungary

Received 20 September 2010; revised 8 December 2010; accepted 8 January 2011

Available online 13 January 2011

B redistribution in a B-implanted polycrystalline NiSi layer has been investigated using atom probe tomography and secondary ion mass spectrometry. The B accumulations observed at the SiO₂/NiSi interface and in the NiSi bulk are due to B clustering. B cluster formation at these two locations is shown to have a major impact upon the entire B distribution observed after annealing. The formation of B clusters in the NiSi bulk may be due to implantation-related defects.

© 2011 Acta Materialia Inc. Published by Elsevier Ltd. All rights reserved.

Keywords: Ni-silicides; Implantation; Boron; Cluster

Interfaces are playing an increasing role in micro-electronic device performance due to the small thickness of the material layers involved in device fabrication processes. For example, impurity distribution engineering in silicides is considered to be an essential way to improve the electrical properties of silicide/silicon [1–4] and silicide/oxide [5–12] interfaces. In particular, dopant segregation at these interfaces may improve device function significantly [1–12]. Many studies have been devoted to understanding and controlling dopant redistribution in silicides during the reaction of a metal with doped Si [1–4,13–16] in order to improve device performance. However, very few studies have been devoted to dopant (or impurity) implantation in silicide with the same goal. The majority of these latter studies have focused on the use of implanted silicides as diffusion sources into silicon [17]. Silicide implantation increases the complexity of the process. However, this route should not be neglected. Because of the persistent reduction in contact surface areas, it is important to investigate all solutions that can allow the production of high-quality contacts on devices. Furthermore, many of the dopant properties of silicides are still unknown or not well understood, such as dopant solubility, dopant diffusion and dopant interactions with implantation defects.

Recently, we studied B and As diffusion in Ni₂Si and NiSi [16,18]. NiSi is the most used silicide in sub-90 nm technologies. B diffusion was shown to be complicated by unexpected accumulations of B atoms in the bulk of the silicide layer and at the SiO₂/NiSi interface. In the bulk, the B accumulation was shown to form a Gaussian distribution located 20 nm deeper than the implanted B distribution. A strong B accumulation at the SiO₂/NiSi interface was observed during annealing, leading to B atom diffusion for concentrations higher than the B solubility limit in NiSi. In this article, we further investigate B redistribution in implanted NiSi using laser-pulsed atom-probe tomography (LP-APT). The post-annealing Gaussian distribution of B atoms observed via secondary ion mass spectrometry (SIMS) in the bulk of NiSi is shown by LP-APT to be due to B clustering. This effect is expected to be related to implantation-induced defects. X-ray diffraction (XRD) spectra obtained on as-implanted samples present the signature of implantation-mediated strain. However, transmission electron microscopy (TEM) did not highlight any defects or amorphous regions in the as-implanted samples. The B accumulation at the SiO₂/NiSi interface is shown to be due to B clustering, and not due to B interface segregation. LP-APT measurements suggest that the B solubility limit in NiSi is between 0.045 and 0.12%, corresponding to an NiSi bulk concentration between 3.74×10^{19} and 1×10^{20} at cm⁻³.

* Corresponding author. E-mail: alain.portavoce@im2np.fr

The sample was produced by successively depositing on a Si(001) substrate a 30 nm thick SiO₂ layer at 730 °C by low-pressure chemical vapor deposition (LPCVD), a 150 nm thick Si layer at 550 °C by LPCVD, a 73 nm thick Ni layer at room temperature by magnetron sputtering, and finally a 20 nm thick SiO₂ layer at 380 °C by LPCVD. After the deposition, the sample was annealed at 700 °C for 2 h in order to stabilize the grains of the polycrystalline silicide layer formed from the reaction of Si and Ni between the two Si oxide films. Rutherford backscattering measurements (He⁺ beam of 2.5 MeV) and XRD measurements showed that only the NiSi compound was present at the end of the fabrication process, and a TEM cross-section view of the sample showed an 180 nm thick polycrystalline layer made of columnar grains having an average width of 150 nm (Fig. 1a). After fabrication, a B dose of 5×10^{15} at cm⁻² was implanted in the sample through the 20 nm thick Si oxide layer using a beam energy of 18 keV. Then the sample was annealed at 550 °C for 1 h under vacuum ($\sim 10^{-7}$ Torr) and analyzed by LP-APT. LP-APT analyses were performed using an Imago LEAP 3000X HR microscope in the pulsed laser mode. The analyses were carried out at 45.9 K, with a laser pulse frequency of 200 kHz, using a laser power between 0.67 and 0.76 nJ, corresponding in our setup to a Si²⁺ and Si⁺ ion ratio between 400 and 50. The sample preparation for LP-APT was performed using a dual-beam FEI Helios focused ion beam (FIB). B concentration profiles were measured in the sample by SIMS using a 3 kV Cs⁺ ion primary beam. TEM observations were performed using a Philips CM-20 microscope (200 kV electron beam).

Figure 1a presents a TEM cross-section view of the as-implanted sample. Neither amorphous regions nor obvious defects can be seen. However, Figure 1b shows that the XRD spectrum acquired after implantation is different from the spectrum obtained after annealing at 550 °C for 1 h. After implantation, each of the XRD peaks of the NiSi lattice are doubled. One of the twin

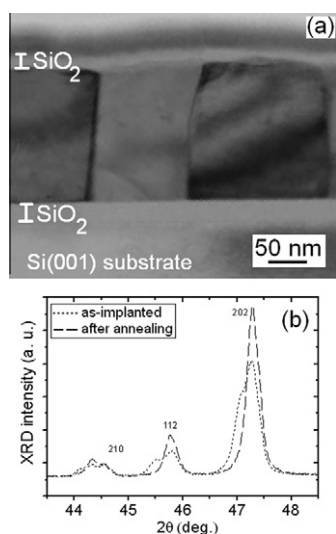


Figure 1. (a) TEM cross-section image of the polycrystalline NiSi layer after implantation of 5×10^{15} B at cm⁻² at 18 keV. (b) XRD spectra acquired after B implantation (dot line), and after annealing at 550 °C for 1 h (dashed line).

peaks is found at the correct diffraction angle and presents a higher intensity. The second peak is shifted toward a smaller angle, which corresponds to an increase in the inter-atomic plane distance due to the implantation-mediated introduction of interstitials in the NiSi lattice [19,20]. After annealing, the strain-related peaks vanished. One can note that the surface area of the twin peaks before annealing is about the same as the surface area of the single peaks after annealing.

Figure 2 presents LP-APT measurements performed after annealing the sample at 550 °C for 1 h. Figure 2a and b corresponds to the three-dimensional (3-D) view of the same volume ($92 \times 92 \times 157.5$ nm³). Each point is an atom. Figure 2a shows 100% B (dark blue) and O (light blue) atoms and Figure 2b shows 1% Si (black) and Ni (green) atoms, as well as 30% O (light blue) atoms. Figure 2c presents a cross-section view (20 nm thick slice) of the same sample. The black isoconcentration surface materializes the interface between the surface SiO₂ layer and the NiSi film; it corresponds to an Si concentration of 30%. The pure Ni layer (Ni cap) on top of the Si oxide was deposited on the sample after the heat treatment, in order to prepare the sample by FIB for LP-APT measurements. Despite the correct atomic Ni/Si ratio (~ 0.5) being found in the silicide, the Si/O ratio measured in the Si oxide did not correspond to the expected value of 0.33. The Si oxide layer was found to have a thickness of about 10 nm and a composition varying between 15 and 33%. We believe that this is due to artifacts related to the difficulty in evaporating this high-field oxide layer in our LP-APT conditions. B accumulations are observed at the SiO₂/NiSi interface and in the bulk of the sample at a depth of ~ 50 nm from the silicide surface. They are shown in

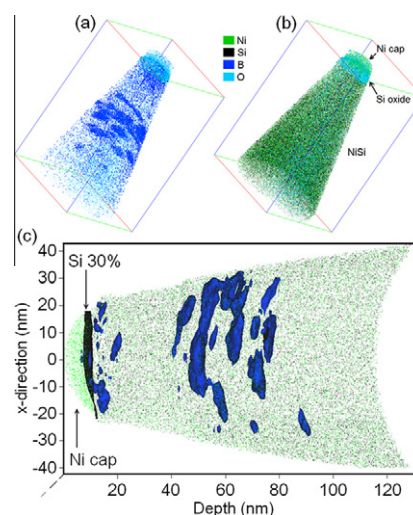


Figure 2. LP-APT analyses performed on the B-implanted NiSi sample after annealing at 550 °C for 1 h. 3-D view of a $92 \times 92 \times 157.5$ nm³ volume (each dot is an atom) showing 100% B (dark blue) and O (light blue) atoms (a) and 1% Si (black) and Ni (green) atoms (b). Cross-section view of a 20 nm thick slice (c), the black isoconcentration surface corresponding to an Si concentration of 30% (SiO₂/NiSi interface) and the blue isodensity surfaces corresponding to a B density of 0.65 B at nm⁻³ (clusters). (For interpretation of the references to color in this figure legend, the reader is referred to the web version of this article.)

Figure 2c using blue isodensity surfaces, corresponding to a density of $0.65 \text{ B at nm}^{-3}$.

Figure 3 presents the comparison between two 1-D B composition profiles vs. depth obtained from two different LP-APT measurements and a SIMS profile obtained in the same sample, after annealing. Each data point at a given depth in the SIMS profile corresponds to a composition averaged over a $60 \times 60 \mu\text{m}^2$ surface. However, the composition given vs. depth in the LP-APT profiles corresponds to a composition averaged over a $30 \times 30 \text{ nm}^2$ surface, so that the statistic in the LP-APT profiles is $\sim 4 \times 10^3$ times lower than that in the SIMS profiles. Consequently, the averaged compositions given by LP-APT are expected to fluctuate around the composition given by SIMS, describing the composition inhomogeneities of the sample.

Three regions are specified in Figure 3. Region I corresponds to the surface Si oxide layer. A high B signal is given by SIMS but, as is well known, this signal may correspond to an artifact due to a different matrix effect between SiO_2 and NiSi (i.e. a different B ionization rate) [21]. No B was detected by LP-APT in this region, confirming that the high B signal in the SIMS profile may arise from B concentrations lower than the detection limit of LP-APT measurements, and enhanced by SIMS matrix effects. The general shape of the APT profiles in regions II and III are in good agreement with the SIMS profile. However, despite the B concentration levels in the SIMS and APT profiles being in agreement in region III (considering the possible statistic deviations discussed earlier), the B concentration is about five times higher in the SIMS profile compared to the APT profile in region II. This could be due to the well-known atom-mixing effect due to ion bombardment during SIMS measurement [22]. Indeed, despite the concentration plateaus in the calibrated SIMS profiles being accurate, the decreasing slopes in the SIMS profiles result from the combination of the real profile in the sample and an artifact slope related to analyzed atoms being pushed deeper into the sample at a constant rate by the incident ion beam. Furthermore, as mentioned earlier, APT observations are local measurements, and are more sensitive to inhomogeneities. For example, in region III, the APT signal presents variations in concentration that are due to B clusters in this region. These variations are smoothed if two APT profiles are superimposed, showing that the concentration distribution due to the B

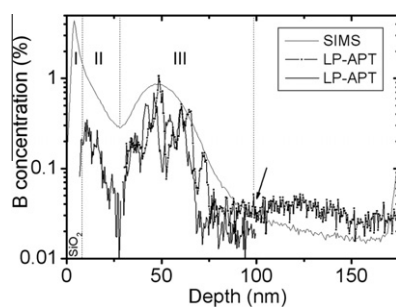


Figure 3. Comparison between the B SIMS profile (thin solid line) and 1-D B concentration profiles obtained in two different LP-APT analyses (thick solid line and line plus dot symbols) performed on the same B-implanted NiSi layer annealed at $550 \text{ }^\circ\text{C}$ for 1 h.

clusters is similar to the Gaussian distribution observed in the SIMS profile. In the same way, the difference in concentration between SIMS and APT in region II may result from sample inhomogeneities. For example, no grain boundaries (GBs) were observed in our APT volumes. However, B diffuses in GBs under our annealing conditions [16], and an increase in the concentration of B should be observable in and around GBs. Consequently, our APT measurements were located in grains (grain average width of 150 nm compared to an average field of view of 60 nm for APT analyses), thus the concentration of B due to its diffusion in GBs is missing in the APT profiles, explaining the difference between the SIMS and the APT. More specifically, as the B concentration in region III is mainly due to B clusters located in the bulk, the SIMS and APT profiles can be close in this region; however, as the B profile in region II is due to B diffusion, the contribution of GB diffusion in this region is expected to be important in the SIMS profile whereas it is inexistent in the APT profiles. Beyond region III, the arrow indicates the depth for which the APT signal corresponds to noise only (no B peak in the mass spectrum).

Considering the shape of the B accumulations observed by LP-APT (Fig. 2a and c) and the B diffusion profiles vs. temperature from Ref. [16], as well as B–Si and B–Ni atomic interactions [23], the B accumulations appear to result from B clustering. Indeed, atom segregation in defects (surface, interface, dislocations, etc.) usually occurs in regions of about 2–3 atomic planes ($\sim 0.5 \text{ nm}$), and increases with bulk concentration and decreases with temperature increases [24]. This is in contrast to our observations. For example, in Figure 2c, B segregation at the SiO_2/NiSi interface is expected to be continuous along the interface and to correspond to a significant increase in B concentration for a depth lower than 1 nm . However, it is reasonable to assume that the B segregation process precedes B clustering on defects.

In summary, APT analyses show that (i) the Gaussian distribution formed during annealing in NiSi bulk is due to B cluster formation; (ii) the B accumulation at the SiO_2/NiSi interface is due to the formation of B cluster, and not to B interface segregation; and (iii) no B cluster was seen between the SiO_2/NiSi interface and the Gaussian distribution, showing that in region II the B distribution results from B diffusion. Furthermore, the examination of the B concentration around the B clusters gives a B content in the NiSi matrix of between 0.045% and 0.12% , which corresponds to an NiSi bulk concentration of between 3.7×10^{19} and $1 \times 10^{20} \text{ at cm}^{-3}$, which is quite similar to the B solubility limit that we previously determined ($\sim 3 \times 10^{19} \text{ at cm}^{-3}$) considering mobile B atoms in SIMS measurements [16]. The cluster formation at the SiO_2/NiSi interface is not surprising as heterogeneous nucleation is generally favored, and interfaces usually contain defects. However, the cluster formation in the bulk is not well understood. The cluster location at a specific depth ($\sim 50 \text{ nm}$ in Fig. 3) and the Gaussian signature (Fig. 3) suggest that B clusters nucleate on implantation-induced defects.

Figure 4 presents experimental B profiles measured by SIMS in the as-implanted sample and after annealing, as well as simulated profiles, obtained using the “Stopping

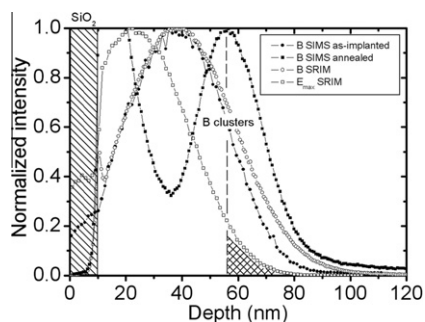


Figure 4. Comparison between SIMS profiles (solid symbols) and SRIM simulated profiles (open symbols).

and Range of Ions in Matter” (SRIM) software, corresponding to the B implantation profile and the energy distribution (E_{\max}) transmitted to the matrix atoms during implantation. The B distribution after implantation is correctly simulated by SRIM; however, the maximum of the Gaussian energy distribution transmitted to the matrix atoms, which indicates the location where the displacement of matrix atoms is maximum (possible amorphization), does not correspond to the location of the B clusters. Nevertheless, one can note that the maximum of the B cluster distribution is located in the tail of the implantation transmitted energy distribution.

The defects triggering B clustering in NiSi bulk may result from the redistribution of implantation defects during annealing (diffusion and agglomeration of interstitials as suggested by XRD measurements in Fig. 1b). For example, one can note that the maximum of E_{\max} is located close to the SiO₂/NiSi interface (about 10 nm away; see Fig. 4). As was shown for the SiO₂/Si interface [25], the SiO₂/NiSi interface may provide a high rate of interstitial recombination, allowing for the recombination of the majority of the implantation-mediated interstitials corresponding to the maximum of E_{\max} . However, the implantation-mediated interstitials located in the tail of E_{\max} , being far from the two SiO₂/NiSi interfaces, may agglomerate and form defects during annealing [26].

A credible scenario can be proposed to explain the complex SIMS profiles obtained in B-implanted NiSi samples after annealing [16]. During annealing, heterogeneous B cluster nucleation occurs at both the SiO₂/NiSi interface and on implantation-related defects in the NiSi bulk. These two sites act as B atom sinks, and prevent cluster formation in between due to the difference in nucleation kinetics between heterogeneous and homogeneous nucleation. B atoms diffuse towards these two nucleation centers, allowing for the growth of B clusters, which explains the observation of B diffusion for concentrations above the usual solubility limit in region II [16]. Deeper than region III, the conventional downhill B diffusion is observed [16].

In conclusion, B redistribution during thermal annealing in B-implanted polycrystalline NiSi has been studied using APT and SIMS measurements. B atoms form clusters via heterogeneous nucleation on defects at the SiO₂/NiSi interface, and in the bulk of the NiSi film deeper than the B-implanted distribution. After

cluster nucleation, B atoms diffuse between the two nucleation centers supplying B cluster growth, and towards the bottom of the layer via Fickian diffusion. In our annealing conditions, B cluster growth at heterogeneous nucleation centers is favored compared to homogeneous bulk nucleation of B cluster.

- [1] Q.T. Zhao, U. Breuer, E. Rije, St. Lenk, S. Mantl, Appl. Phys. Lett. 86 (2005) 062108.
- [2] M. Sinha, E.F. Chor, Y.-C. Yeo, Appl. Phys. Lett. 92 (2008) 222114.
- [3] H.-S. Wong, L. Chan, G. Samudra, Y.-C. Yeo, Appl. Phys. Lett. 93 (2008) 072103.
- [4] S.F. Feste, J. Knoch, D. Buca, Q.T. Zhao, U. Breuer, S. Mantl, J. Appl. Phys. 107 (2010) 044510.
- [5] M.A. Pawlak, J.A. Kittl, O. Chamirian, A. Veloso, A. Lauwers, T. Schram, K. Maex, A. Vantomme, Microelectron. Eng. 76 (2004) 349.
- [6] H.C. Wen, J. Liu, J.H. Sim, J.P. Lu, D.L. Kwong, Electrochem. Sol.-State Lett. 8 (2005) G119.
- [7] M. Copel, R.P. Pezzi, C. Cabral Jr., Appl. Phys. Lett. 86 (2005) 251904.
- [8] J. Liu, D.L. Kwong, Appl. Phys. Lett. 88 (2006) 082105.
- [9] J. Liu, D.L. Kwong, Appl. Phys. Lett. 88 (2006) 192111.
- [10] Y. Tsuchiya, M. Yoshiki, A. Kinoshita, M. Koyama, J. Koga, J. Appl. Phys. 102 (2007) 104504.
- [11] Y. Tsuchiya, M. Yoshiki, K. Sekine, T. Saito, K. Nakajima, T. Aoyama, J. Koga, A. Nishiyama, M. Koyama, M. Ogawa, S. Zaima, J. Appl. Phys. 103 (2008) 124503.
- [12] B.-M. Wang, G.-P. Ru, Y.-L. Jiang, X.-P. Qu, B.-Z. Li, R. Liu, Appl. Surf. Sci. 255 (2008) 1744.
- [13] K. Hoummada, D. Mangelinck, C. Perrin, P. Gas, V. Carron, P. Holliger, E. Ziegler, Microelectron. Eng. 83 (2006) 226.
- [14] K. Hoummada, D. Mangelinck, C. Perrin, V. Carron, P. Holliger, J. Appl. Phys. 104 (2008) 024313.
- [15] O. Cojocaru-Mirédin, C. Perrin-Pellegrino, D. Mangelinck, D. Blavette, Microelectron. Eng. 87 (2010) 271.
- [16] I. Blum, A. Portavoce, L. Chow, D. Mangelinck, K. Hoummada, G. Tellouche, V. Carron, Appl. Phys. Lett. 96 (2010) 054102.
- [17] Y.H. Ku, S. Lee, D.L. Kwong, P. Chu, Appl. Phys. Lett. 54 (1989) 1684.
- [18] I. Blum, A. Portavoce, D. Mangelinck, R. Daineche, K. Hoummada, J.L. Lábár, V. Carron, C. Perrin, J. Appl. Phys. 104 (2008) 114312.
- [19] J. Dudognon, Ph.D. Thesis, Université d’Orléans, 2006.
- [20] N. Cherkashin, S. Reboh, F. Houdellier, A. Claverie, M.J. Hÿtch, oral communication, E-MRS 2010 Spring Meeting, Symposium Q: Quantitative Electron Microscopy for Research and Industry.
- [21] M. Meuris, W. Vandervorst, J. Jackman, J. Vac. Sci. Technol. A9 (1991) 1482.
- [22] A. Portavoce, N. Rodriguez, R. Daineche, C. Grosjean, C. Girardeaux, Mater. Lett. 63 (2009) 676.
- [23] T.B. Massalski, H. Okamoto, P.R. Subramanian and L. Kacprzak (Eds.), Binary Alloy Phase Diagrams. Materials Park, OH: ASM International, 1996.
- [24] G. Tréglia, B. Legrand, F. Ducastelle, A. Saül, C. Gallis, I. Meunier, C. Mottet, A. Senhaji, Comp. Mater. Sci. 15 (1999) 196.
- [25] E.M. Bazizi, A. Pakfar, P.F. Fazzini, F. Cristiano, C. Tavernier, A. Claverie, N. Zographos, C. Zechner, E. Scheid, Thin Solid Films 518 (2010) 2427.
- [26] B. Colombeau, N.E.B. Cowern, F. Cristiano, P. Calvo, N. Cherkashin, Y. Lamrani, A. Claverie, Appl. Phys. Lett. 83 (2003) 1953.